Transparent semiconductor–polymer hybrid films with tunable optical properties†

Y. Martínez,[ad] J. Retuert,*[a] M. Yazdani-Pedram[b] and H. Cölfen*[c]

Received 20th September 2006, Accepted 1st December 2006
First published as an Advance Article on the web 22nd December 2006
DOI: 10.1039/b613694j

Size confined CdS nanoparticles with controlled size and narrow particle size distribution were synthesized in transparent adhesive polyelectrolyte films, which are composed of chitosan (CHI), poly(monomethyl itaconate) (PMMI) and silica (SiO_2) in variable amounts. This room temperature synthesis in an aqueous environment avoids the toxic and high temperature conditions usually associated with the synthesis of high quality semiconductors. The semiconductor particle size could be controlled *via* the Cd^{2+} concentration and the amine groups of chitosan were identified to be of importance for the coordination of the semiconductor. The films were characterized by UV-Vis and fluorescence spectroscopy, transmission electron microscopy, X-ray diffraction, X-ray photoelectron spectra and the adsorption behavior of Cd^{2+} to the films was characterized by Langmuir and Freundlich isotherms.

Introduction

The incorporation of functional nanoparticles into polymer matrices has received increasing attention both from the scientific as well as the industrial viewpoint because such hybrid materials are at a fusion point between the already well known and established processability of polymer films or complexes and the functions of the incorporated nanoparticles. In that respect, the unique optical or electronic properties of inorganic semiconductors are of special interest. II/VI Semiconductors are an example of a semiconductor exhibiting quantum confinement in the 1–20 nm range. In particular, CdS is a well studied system,[1] as CdS nanoparticles generally show the quantum confinement effects for particles in the size range of 1–6 nm.[2] Tuning the size of the incorporated semiconductor nanoparticles allows for a tunable change in optical and electronic properties as was revealed by a multitude of theoretical and experimental studies on quantum sized semiconductor nanoparticles.[3–5] A narrow size distribution of the incorporated semiconductor particles is of pivotal importance, as otherwise the defined quantum confinement effects like band gaps are essentially smeared out, so a strong demand exists to synthesize monodisperse but nevertheless size tunable semiconductor nanoparticles inside processable polymer films.

The common way towards high quality nanocrystalline semiconductor nanoparticles involves surfactant mediated templating techniques.[6,7] These processes generally employ the hot injection method, involving the addition of a precursor solution to a hot liquid, often consisting of molten surfactants, in a temperature range of 200–300 °C,[8] procedures that are far away from being economically attractive. However, milder reaction routes to CdS in water and in the presence of block copolymers were also reported[9] and point out the possibility that an aqueous route towards high quality semiconductor–polymer hybrid films should exist. Another alternative way to produce nanoparticle–polymer composites is the use of a polymerizable surfactant to transfer water-soluble nanocrystals into a monomer solution which is then polymerized.[10]

The general principle in the synthesis of optical composites involves an intimate incorporation of the material with optical properties inside a manageable matrix. In this way for example, it is possible to incorporate semiconductor quantum particles in matrices such as polymers, blends, glasses and ceramics.[11–17] Using this approach the nanoparticles are in a condensed phase, which is necessary for multiple applications that involve portable and robust devices.

A particularly interesting possibility to induce monodisperse semiconductors into a polymer film would certainly be the incorporation of pre-fabricated monodisperse semiconductor nanoparticles, which are meanwhile synthetically available by a variety of methods[18,19] and in a variety of morphologies.[20]

Via this pathway, a number of polymer–semiconductor composites could be prepared.[21,22] However, a phase compatibilization step has to be involved to link the pre-fabricated inorganic material to the polymer matrix in addition to the high temperature and usually toxic reaction environment required for the synthesis of monodisperse semiconductor nanoparticles.

The essential drawback of such strategy is that a compatibilizing molecule has to be applied to facilitate incorporation

[a]*Center for Advanced Interdisciplinary Research in Materials (CIMAT) and Facultad de Ciencias Físicas y Matemáticas, Universidad de Chile, Av. Beaucheff 850, Casilla 2777, Santiago, Chile. E-mail: jretuert@dqb.uchile.cl; Fax: ++56-2-6994119; Tel: ++56-2-6784226*
[b]*Center for Advanced Interdisciplinary Research in Materials (CIMAT) and Facultad de Ciencias Químicas y Farmacéuticas, Universidad de Chile, Olivos 1007, Casilla 233, Santiago, Chile*
[c]*Max-Planck Institute of Colloids and Interfaces, Colloid Chemistry, Research Campus Golm, Am Mühlenberg, D-14424 Potsdam, Germany. E-mail: Coelfen@mpikg.mpg.de; Fax: ++49-331-567-9502; Tel: ++49-331-567-9513*
[d]*Steacie Institute for Molecular Sciences, National Research Council of Canada, Ottawa, Ontario K1A 0R6, Canada*
† Electronic supplementary information (ESI) available: Images of CdS-hybrid film composites with different CHI : SiO_2 : PMMI molar ratios. See DOI: 10.1039/b613694j

of the semiconductor nanoparticles into the polymer membrane without prior aggregation, which is often a hydrophilic–hydrophobic transition. As an alternative, a hydrophilic environment can be sought for the incorporation of the semiconductor nanoparticles. An example of this strategy is the incorporation of semiconductor nanoparticles into polyelectrolyte multilayers *via* layer by layer (LBL) assembly driven by electrostatic attractions between the layer forming components.[23–25]

However, a LBL technique requires multiple deposition and washing steps and in addition requires the preformed semiconductor particles, which have the above mentioned synthesis drawbacks.

As a consequence, it seems best to directly synthesize the semiconductor particles in a controlled fashion directly within the polymer film matrix. The latter can then be tuned towards the envisaged coating application. Several examples of this strategy were already reported in the literature but the polymer films are either soluble in water like poly(ethylene oxide)[26–30] or the CdS particles are prepared by thermolysis of a precursor[31] or the polymer itself as a sulfur source.[32]

Therefore, several demands towards optically functional coating films can be defined, namely insolubility, transparency, defined optical and electronic functionality and tunable semiconductor particle size.

An additional requirement is that the incorporated inorganic nanoparticles have to be prevented from degradation like photocorrosion in the case of CdS, which is a problem with this type of oxidation sensitive semiconductor and was just recently overcome by a reductive polymer layer in the form of an electron donating polyamine layer.[9] The above restrictions indicate the limits of a top down approach towards functional semiconductors embedded in a functional polymeric phase.

We have therefore explored the bottom up approach and studied the *in situ* formation of semiconductor nanoparticles of CdS in organic–inorganic hybrid films. The selected hybrid films are composed of chitosan (CHI), poly(monomethyl itaconate) (PMMI) and silica (SiO_2). These films are transparent and they don't disintegrate in aqueous solutions as they are able to the form interpenetrated networks.[33] Also they are strongly adhering to glass and graphite surfaces suggesting a coating application for these films. It is possible to modulate the concentration of the different functional groups by varying the composition of the films. The idea of a functional organic–inorganic hybrid film coating exploits the introduction of CdS nanoparticles to take advantage of the physical properties of the ternary films CHI–SiO_2–PMMI and in this way, for example, to obtain an adhesive coating with special optical properties as a function of the semiconductor nanoparticle size.

Experimental section

Chitosan (high molecular weight) was purchased from Aldrich (Milwaukee, USA). The degree of deacetylation and the molecular weight were determined according to the procedures described by Rinaudo and Domard.[34] The degree of deacetylation was estimated as 83% by titration of amino groups, and the weight average molecular weight was determined as 3.55×10^5 g mol^{-1} by combined viscosity–light scattering measurements. CHI was used as a 1% solution in dilute formic acid (5%). The siloxane sol was prepared starting from tetraethoxysilane (TEOS) (Aldrich) and with formic acid as catalyst. The initial molar composition was TEOS : H_2O : formic acid : EtOH = 1 : 1 : 0.01 : 10. Monomethyl itaconate and PMMI were prepared as previously reported.[35] The apparent number and weight average molecular weights ($M_n = 1.1 \times 10^5$ g mol^{-1}, $M_w = 1.6 \times 10^5$ g mol^{-1}) were determined by gel permeation chromatography (GPC) using a Waters HPLC model 600 equipped with a differential refractive index detector model 410 and a Shodex KB-803 GPC column. The GPC column was calibrated by using polyethylene oxide standards from Waters (part No. WAT011572) having molecular weights in the range 2.4×10^4–8.5×10^5. The mobile phase was 0.25 M NaCl solution and the flow rate for analysis was 1 mL min^{-1} at 25 °C.

Film preparation

The hybrid films were prepared as described in ref. 33. Siloxane sol, PMMI, ethanol solutions and chitosan solutions were mixed in the appropriate ratios to have CHI : SiO_2 : PMMI ratios from 1 : 1 : 0.3 to 0.3 : 1 : 0.5 (Table 1). Then the mixture was stirred for 24 h. For all the compositions the pH values of the mixtures were around 2.7–2.75. The SiO_2 : CHI : PMMI molar ratio of the samples was calculated from the molecular weight of the monomeric unit of CHI (168.1 g mol^{-1}) considering the acetylation degree of 17% and the molecular weight of the PMMI repeating unit (144 g mol^{-1}). The amount of siloxane precursor was calculated by considering that 1 mol of TEOS after total hydrolysis produces 1 mol of SiO_2.

Preparation of CdS-Hybrid film composites

In order to obtain hybrid films with different compositions (Table 1) the precursor solutions were cast on quartz slides and dried at ambient temperature for two weeks. In a typical procedure the films (15–25 mm thick) were immersed in pH 9 buffer solution from Merck (Boric acid, KCl and NaOH) for three hours, then they were soaked in 10 mL of 2 mM $CdCl_2$ solutions for 24 h at room temperature, rinsed with deionized water and then immersed in 10 mL of 2 mM Na_2S solution for 24 h. The resulting pale yellow transparent films were rinsed again, dried at room temperature and then characterized. The influence of the concentration of the $CdCl_2$ and Na_2S solutions (0.05, 0.1, 0.25, 0.5, 0.7, 1, 2 and 3 mM) was also studied.

Table 1 Properties of CdS particles incorporated in hybrid films of different compositions. $CdCl_2$ and Na_2S 2 mM. λ_a = position of the absorption edge (band gap) used for the determination of the particle size according to ref. 37, λ_b = position of the exciton peak

Sample	CHI : SiO_2 : PMMI/moles	λ_a/nm	λ_b/nm	Mean diameter[a]/Å
CSP1	1 : 1 : 0.3	435	357	31
CSP2	0.7 : 1 : 0.3	440	357	32
CSP3	0.6 : 1 : 0.3	440	357	32
CSP4	0.4 : 1 : 0.5	499	—	58
CSP5	0.3 : 1 : 0.5	540	—	⩾100

[a] According to UV-visible spectroscopy.

Characterization of the CdS-hybrid films composites

UV-Vis spectra were recorded using a UV-Vis spectrophotometer (Hewlett Packard) with a setup where the light could directly pass through the prepared films The X-ray photoelectron spectra (XPS) were obtained with a Physical Electronics 1257 system with a hemispheric analyzer using Al Kα radiation (hv = 1486.6 eV) at room temperature. The measurements were made by collecting the photoelectrons at 0° with respect to the normal to the sample surface. All XPS peaks were referred to the position of the C (1s) peak at 284.5 eV. Emission spectra were recorded on a Spex Fluorolog-2 spectrophotometer. The samples were measured in the front face mode with an excitation wavelength λ_{exc} of 350 or 360 nm as will be specified. The films were positioned at a 22.5° angle to the incident excitation source. Transmission electron microscopy (TEM) was performed on a DMS 940 A (Carl Zeiss, Jena) microscope operating at 120 kV. The samples were prepared by thin slicing the film at a thickness of *ca*. 100 nm with a Leica ultracut UCT ultramicrotome and placing the thin slice on a copper TEM grid.

Results and discussion

We previously described the synthesis of new polymeric organic–inorganic hybrid films based on silica and a polyelectrolyte complex between CHI and PMMI.[33] The products can be prepared as self-supported homogeneous and transparent films or deposited as well adhering coatings on a variety of surfaces like glass, graphite, steel, *etc*. Intermolecular hydrogen bonding stabilizes this self-assembled structure. Transmission electron microscopy and atomic force microscopy were used to examine the homogeneity of the ternary polymer hybrids films (CHI–PMMI–SiO_2). The results showed a nanometer scale dispersion of the phases.[33]

In these films it is possible to control the concentration of amine and carboxylic groups and thereafter change the ionic properties by varying the composition of the organic components. Thereafter, the combination of the adhering properties of the ternary CHI–SiO_2–PMMI films and their optical transparency with their ability to incorporate inorganic particles may lead to interesting new functional materials. The use of gel structures for the precipitation of well dispersed magnetite particles was already demonstrated.[36] The functional groups potentially useful for the coordination of heavy metal ions are the amine groups of chitosan which can coordinate the Cd^{2+} ions by complexation, and the carboxylate groups of PMMI that could fix the Cd^{2+} ions as counterions [$(R–COO^-)_2Cd^{2+}$] by means of an electrostatic interaction. The coordinated Cd^{2+} ions then serve as nuclei and material depots for further growth of CdS nanoparticles after the films were exposed to sulfide ions.

As can be seen in Fig. S1 (ESI†) the formation of CdS is manifested by a coloration of the films that goes from pale yellow to yellow, depending on the composition, however the films remain transparent. The UV-Vis spectra provide a convenient way to observe the formation of the CdS particles with a size of a few nm, as well as to determine their size *via* the position of the band gap,[37] as the transparency of the films minimizes the disturbance of the absorption spectra by light scattering phenomena. In the absence of CdS, the hybrid films with compositions as shown in Table 1, do not show absorption at wavelengths higher than 280 nm.

The formation of CdS is proven by the development of absorption in the visible region of the spectrum (Fig. 1). When the films are not immersed in a pH 9 buffer solution before Cd^{2+} is introduced, the absorption is fairly low. As is well known, the onset of the absorption band in the UV-Vis spectrum of semiconductor nanoparticles is attributed to the band gap absorption, and this will be blue-shifted relative to the bulk (515 nm) due to a quantum size confinement effect.[37,38]

As shown in Fig. 1 the UV thresholds of all samples, except CSP5, are blue-shifted relative to the bulk CdS, indicating the formation of CdS nanoparticles. By increasing the CHI amount in the films, the absorption edge of the obtained CdS nanoparticles was decreased gradually from 540 to 435 nm, suggesting that smaller CdS nanoparticles (3 nm) were produced at higher CHI concentrations. The average particle size was obtained according to the experimental curve of the absorption edge *versus* particle diameter for CdS.[37] These results are summarized in Table 1.

It is worth mentioning that as the CHI amount was increased, besides a decrease in the particle size, the exciton peak (λ_b) became sharper and an even higher energy transition is observed in samples CSP1 and CSP3. These characteristics indicate a narrow particle size distribution. In these films the features of the UV-Vis spectra are similar to the ones obtained for well capped particles synthesized in reverse micelles or arrested precipitation using suitable organic moieties.[9,39] Although there are several examples of CdS nanoparticles synthesized *in situ* in solid matrices or films, usually the UV-Vis spectra do not show these features.[11,12,15,40]

To our knowledge, the exciton peaks in the UV-Vis absorption spectra of CSP1 and CSP3 shown in Fig. 1 are among the sharpest for CdS nanoparticles synthesized *in situ* in a solid matrix indicating the high quality of our samples.[41,42]

As we stated previously, chitosan and PMMI form an interpolymeric complex in the hybrid films. Considering the composition of CSP1, CSP2 and CSP3 a fraction of the amine groups would be involved in the formation of the complex

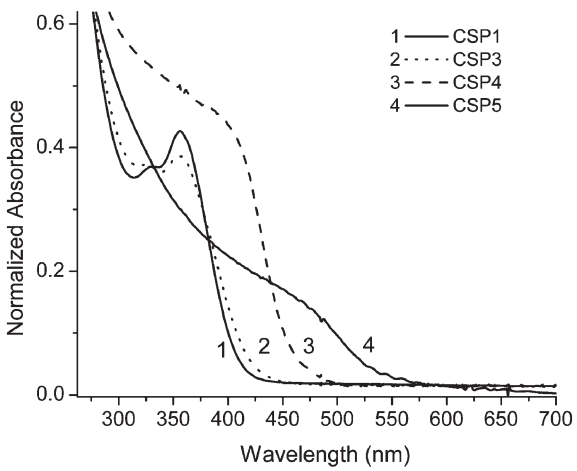

Fig. 1 UV-Vis absorption spectra of CdS nanoparticles formed in hybrid films of different compositions. $CdCl_2$ and Na_2S 2 mM.

while the rest would be available to coordinate the Cd^{2+} ions. This would not be the case for CSP4 and CSP5 where the concentration of amine groups is smaller than the concentration of carboxyl groups.

When increasing the pH, by immersing the films in a pH 9 buffer solution, the amine group, which was protonated due to the initial pH of the CHI solution, became neutral which increases the availability of coordinating groups. A high local concentration of amine groups along the chitosan backbone coordinate the Cd^{2+} ions favoring their incorporation into the films and in this way promote the growth of the CdS nanoparticles formed after reaction with sulfide ions.

In order to investigate the effect of Cd^{2+} and S^{2-} concentration on the formation of the CdS nanoparticles two sets of experiments were carried out where the $Na_2S/CdCl_2$ molar ratio, at different concentrations, was kept either equal to one or bigger than one. Fig. 2(a) shows the absorption spectra obtained for CSP3 when the molar ratio $Na_2S/CdCl_2$ was equal to one. On the other hand Fig. 2(b) shows the absorption spectra obtained when different concentrations of $CdCl_2$ are used (2 mM–0.05 mM), but always keeping the molar ratio $Na_2S/CdCl_2$ larger than one. Table 2 summarises the properties of the CdS nanoparticles formed in each case.

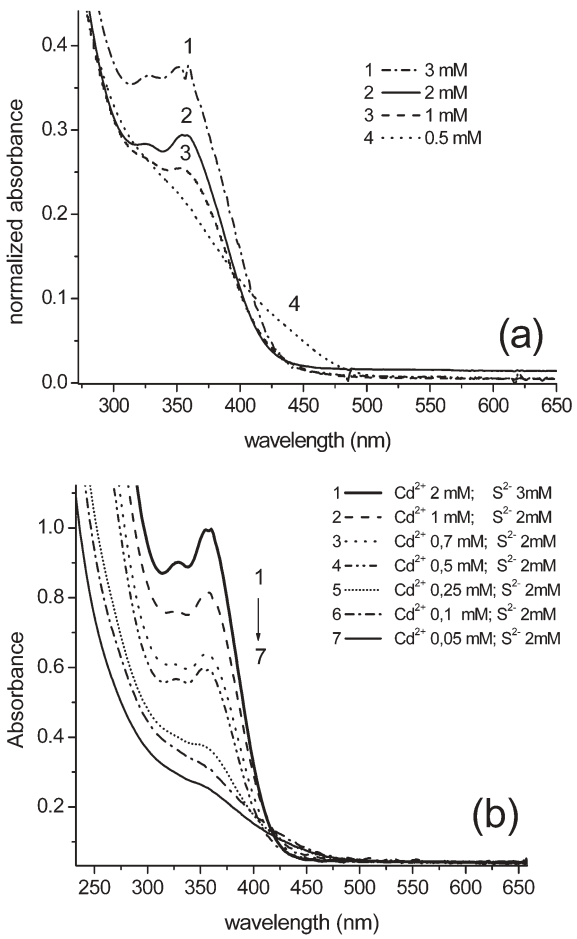

Fig. 2 Absorption spectra of CdS particles generated *in situ* in CSP3. (a) Soaked in solutions with $Na_2S/CdCl_2 = 1$ and different concentrations. (b) Soaked in solutions of different Cd^{2+}concentration, $Na_2S/CdCl_2 > 1$.

Table 2 Properties of the CdS particles generated in CSP3. λ_a = Position of the absorption edge (band gap) used for the determination of the particle size according to ref. 37, λ_b = position of the exciton peak

$CdCl_2$/mM L^{-1}	Na_2S/mM L^{1-}	λ_a/nm	λ_b/nm	Mean diameter/Å[a]
3	3	440	355	32
2	2	445	357	34
1	1	440	357	32
0.5	0.5	487	—	51
2	3	440	357	32
1	2	445	357	34
0.7	2	445	357	34
0.5	2	440	357	32
0.25	2	485	—	51
0.1	1	485	—	51
0.05	1	490	—	54

[a] From absorption spectra.

In general, it is expected that the particle size will decrease when the concentration of $CdCl_2$ is decreased, since it would be equivalent to increasing the concentration of stabilizer groups in addition to less material being available for the particle growth. However, it can be seen in Fig. 2(a) that by decreasing the concentration of the $CdCl_2$ solutions from 1 mM to 0.5 mM ($Na_2S/CdCl_2 = 1$) there is a red-shift of the absorption band corresponding to a significant increase in the particle size from 32 to 54 Å and at the same time the exciton peak disappears. When the concentration is higher than 1 mM, significant variations in the absorption band are not observed. However, the exciton peak gets continuously less pronounced when decreasing the Cd^{2+} concentration from 3 mM to 1 mM indicating an increasing polydispersity of the formed CdS particles.

The behavior observed in Fig. 2(a) could be explained by an altered number of nucleation sites. Decreasing the reactant concentration decreases the supersaturation, so that nucleation takes place in increasing time intervals and the formed particles become more polydisperse. This becomes understandable when the requirements for the formation of monodisperse particles are considered according to the classical paper by LaMer and Dinegar, which shows that a nucleation burst is needed in a short time period followed by growth to obtain monodisperse particles.[43] Obviously, at 0.5 mM Cd^{2+}, a threshold is reached and far less CdS nuclei are formed than at the higher concentrations thus leading to the growth of larger particles. In addition, the nucleation apparently takes place over a larger time interval than before and the previously fixed Cd^{2+} ions as well as the S^{2-} ions have to migrate inside the film to the growing CdS nuclei, which will lead to a broad particle size distribution with the consequent disappearance of the exciton peak.

On the other hand, when the molar ratio $Na_2S/CdCl_2$ is higher than one (Table 2) it can be seen [Fig. 2(b)] that for $CdCl_2$ concentrations equal to or higher than 0.5 mM the absorption onset occurs practically at the same wavelength. This would indicate that there are no significant changes in the average particle size. Comparing the absorption spectra for the Cd^{2+} concentration of 0.5 mM in Fig. 2(a) (0.5 mM S^{2-}) and Fig. 2(b) (2 mM S^{2-}) shows a significant difference in the band

gap position and the exciton peaks. At the higher S^{2-} concentration, the particle nucleation is much more defined and the number of nucleation sites is higher resulting in a smaller particle size. This shows that the amount of free S^{2-} according to the acid–base equilibrium of H_2S ($pK_{a1} = 7$ $pK_{a2} = 12.92$) is the limiting factor rather than that of Cd^{2+} and that the amount of free S^{2-} available for the formation of CdS in the films is limited.

In Fig. 2(b), it can also be seen that an increase in the Cd^{2+} concentration increases the intensity of the absorption, demonstrating the presence of a larger number of CdS nanoparticles in the film, which maintain their narrow size distribution.[44,45] However, when lower $CdCl_2$ concentrations are used (0.25–0.05 mM) there is a red-shift of the absorption onset and at the same time the exciton peak gradually disappears. This result indicates that a critical value of Cd^{2+} concentration exists between 0.25–0.50 mM, above which CdS nanoparticles begin to be formed with a narrow size distribution. Probably, working below the critical limit where there are more NH_2 groups than Cd^{2+} ions, there will be a competition for Cd^{2+} ions. Thus, Cd^{2+} would accumulate in the regions of highest NH_2 density resulting in a rather inhomogeneous particle distribution in the films. Also, as the local distribution of Cd^{2+} is inhomogeneous, the CdS particle size will be heterogeneous and thus a broadening and decrease of the exciton peak is observed until it completely vanishes.

For the smaller particles, there is a second peak at 325–330 nm beside the exciton peak. The presence of two maxima in the absorption band has been previously observed in thioglycerol and polyphosphate stabilized clusters indicating a bimodal size distribution of these.[37,46,47] This observation was only made for very small clusters where the growth did not occur *via* the Ostwald ripening mechanism, typical of particle growth in colloid chemistry.[47] This points towards the presence of very small clusters stabilized by the amino groups of chitosan in our system. It is interesting to remark that after several months no changes in the absorption/emission spectra of the samples was observed indicating that no aggregation process of the particles took place.

Fluorescence spectra of CdS nanoparticles, produced *in situ* in hybrid films of different compositions are shown in Fig. 3. The spectra were recorded at an excitation wavelength of 350 nm. In the absence of CdS the hybrid films revealed no fluorescence. In the functionalized films, the photoluminescence (PL) spectra present Gaussian-like emission bands that are red-shifted from the absorption onset.

The PL spectra of the CdS generated in the hybrid films of different compositions show that with increasing CHI percentage in the film the relatively broad PL band blue-shifts gradually from 577 to 481 nm (Fig. 3). The position of the emission band maximum is related to the CdS nanoparticle size, shifting to higher energies with decreasing particle size.[48–50]

Fig. 4 shows the PL spectra of the CdS generated in the hybrid film CSP3 when different concentrations of $CdCl_2$ are used (2 mM–0.05 mM), and keeping the molar ratio $Na_2S/CdCl_2 > 1$. The spectra were recorded at an excitation wavelength of 360 nm. Under these experimental conditions the PL spectra of the functionalized films show a broad band

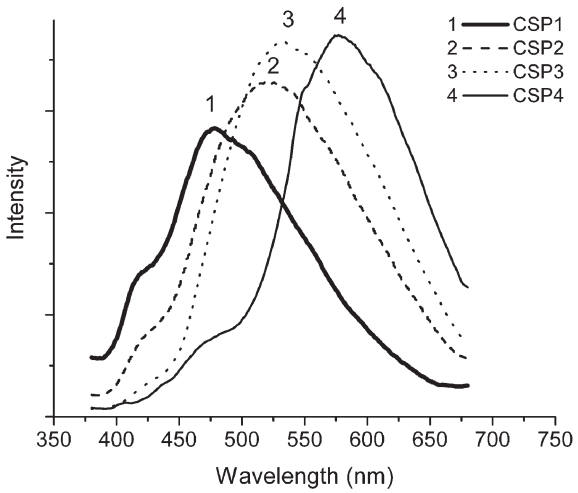

Fig. 3 Fluorescence spectra of CdS particles formed in the hybrid films of different compositions. $\lambda_{exc} = 350$ nm. $CdCl_2$ and Na_2S 2 mM. The sample compositions are given in Table 1.

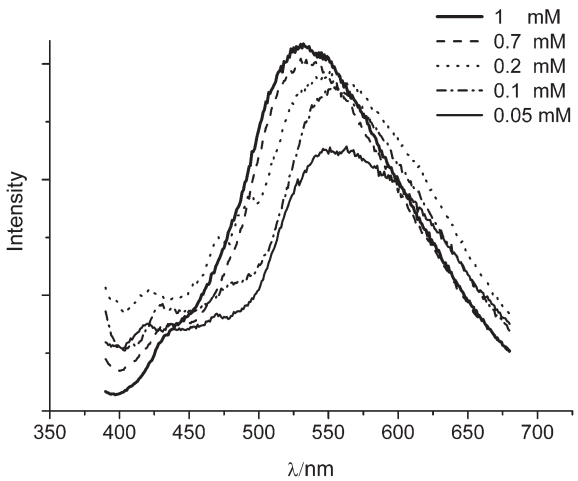

Fig. 4 Fluorescence spectra of CdS particles generated in CSP3. Films were soaked in solutions of different Cd^{2+}concentration, $Na_2S/CdCl_2 > 1$. See Table 2 for sample compositions. $\lambda_{exc} = 360$ nm.

that peaks at 500–560 nm and is red-shifted from the absorption band onset and, as was mentioned previously, it is attributed to a trap-state emission.

In Fig. 4 it can be observed that the broadband maximum shifts to higher wavelengths as the $CdCl_2$ concentration decreases. The maximum is located at 553, 557 & 560 nm for concentrations 0.25, 0.1 and 0.05 mM respectively. At the same time the band gets wider and less symmetrical. This shifting toward higher wavelengths is associated with the formation of bigger particles. On the other hand, when the concentration is higher than 0.5 mM, like 0.7 mM and 1 mM, a blue-shift of the fluorescence maximum is observed being located at 535 nm in both cases. These results again indicate that a critical concentration limit exists for the formation of nanoparticles with a narrow size distribution.

An estimation of the chemical composition of the functionalized CSP3 film was done by X-ray photoelectron spectroscopy (XPS). The results are shown in Fig. 5 where the signals

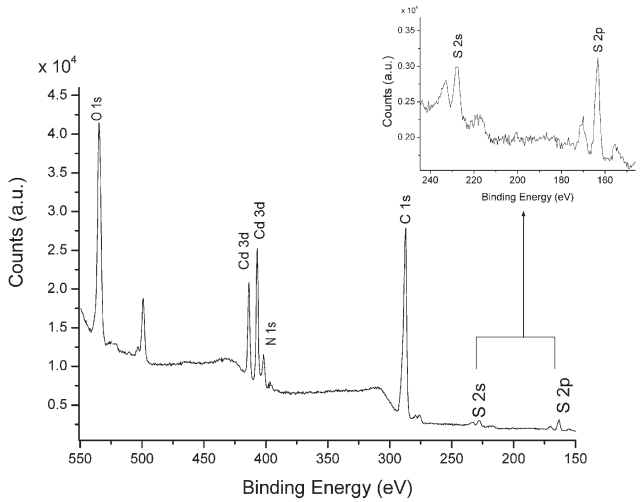

Fig. 5 XPS spectrum of the CSP3 film functionalized with CdS. Signals of S (2s) and (2p) appear in the insert.

corresponding to S (2p) and (2s) are also inserted. The identification was carried out taking into account the binding energies of the elements. The results were as follows: Si (2p) 103.3; S (2p) 162.3; C (1s) 286.2; N (1s) 400,6; Cd (3d5/2) 405.8; Cd (3d3/2) 412.5; O(1s) 533.3 eV. There is also a signal at 497 eV, which was identified as Na. Probably this element was incorporated during the pH treatment of the film and could be present as counterion of the COO^- groups.

Wide-angle X-ray scattering (WAXS) measurements are shown in Fig. 6. Before the functionalization, the hybrid films do not show reflections in the WAXS diffractograms indicating their non ordered structure. For the hybrid–CdS film the diffractogram gave three broad peaks with *d* spacing of 6.50, 3.01 and 2.30 Å. They indicate the introduction of order in the sub-nm range upon CdS formation inside the films, which follows the prior coordination of Cd^{2+} ions to the amino groups of chitosan. The CdS itself is not visible in the WAXS diffractograms due to its low concentration compared to the other components. These results coincide with earlier findings on binary chitosan films exposed to ions.

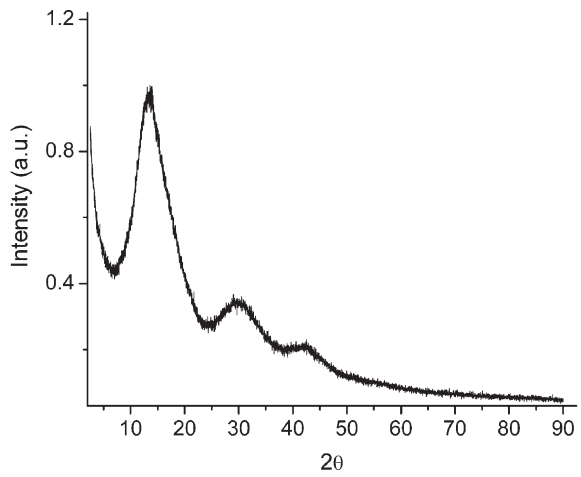

Fig. 6 WAXS diffractogram of CSP3 CdS-hybrid film.

In previous work dealing with binary chitosan–poly(aminopropylsiloxane) (pAPS) films[51] it was found that chitosan sheets are waved and lock up particles of pAPS resulting in an egg-box structure type. When adding salts of Li^+, the amino groups of pAPS coordinate these ions generating an ordered structure in flat layers which was visible in WAXS diffractograms and other techniques. With this in mind, it can be supposed that through the coordination of the Cd^{2+} ions, also a reorientation of amorphous β-chitosan towards the more crystalline α-chitosan can take place.

Transmission electron microscopy (TEM) was used to obtain direct information on the CdS particle size as well as morphology and distribution. Fig. 7 shows TEM images of the nanoparticles generated in CSP3 when using 2 mM (Fig. 7A) and 0.5 mM (Fig. 7C) solutions of $CdCl_2$ and Na_2S. Fig. 7B shows a TEM image of CSP5 when using 2 mM solutions of $CdCl_2$ and Na_2S. It is seen from Fig. 7A that CdS nanoparticles of about 3 nm were randomly distributed on the film. However, in agreement with the estimated values obtained from the absorption spectra, the CdS nanoparticles generated from the 0.5 mM solution were bigger, with an average size of 6 nm and an uneven distribution inside the film (Fig. 7C). On the contrary, in CSP5 the formation of nanoparticles was hardly observed, this could be due to a deficiency of available amino groups, as explained above. Only very few, large particles could be seen. Again, the obtained results agree with those estimated from the UV absorption onset where we observe a dependence of the particle size on the composition of the hybrid films and the concentration of the CdS precursor solutions.

In a two-component system (sorbent and solution) a graph of the solute concentration in the solid phase C_{abs} (mg g^{-1}) can be plotted as a function of the solute concentration in the liquid phase C_{eq} (mg dm^{-3}) at equilibrium. At equilibrium there is a defined distribution of the solute between the liquid and the solid phase, which can generally be expressed by one or more isotherms. Fig. 8 shows the isotherm of the adsorption of Cd^{2+} ions by the CSP3 film.

The results of the Cd^{2+} concentration dependence study were subject to analysis by means of both Langmuir and Freundlich adsorption isotherms. The linearised Freundlich equation, which is used to describe heterogeneous surface energies, fitted the data better than the Langmuir equation with correlation coefficients of 0.99263 and 0.98266 respectively. The following linearised forms of the Langmuir and Freundlich equations were used:

$$C_{eq}/C_{abs} = a_L C_{eq}/K_L + 1/K_L$$

$\log C_{abs} = \log K_F + 1/n \log C_{eq}$ where: C_{abs} = Cd^{2+} adsorbed (mg g^{-1}), C_{eq} = equilibrium concentration in solution (mg L^{-1}), K_F = Freundlich constant (L g^{-1}), $1/n$ = Freundlich exponent, K_L = Langmuir constant (L g^{-1}), a_L = Langmuir constant (L mg^{-1}).

The values of K_F and $1/n$, which are rough measurements of the adsorption capacity and adsorption intensity of the adsorbent, have been determined by the least-square fitting and were found to be 4.1 L g^{-1} and 0.441 L g^{-1} respectively. Processes with values of the Freundlich constant in the range

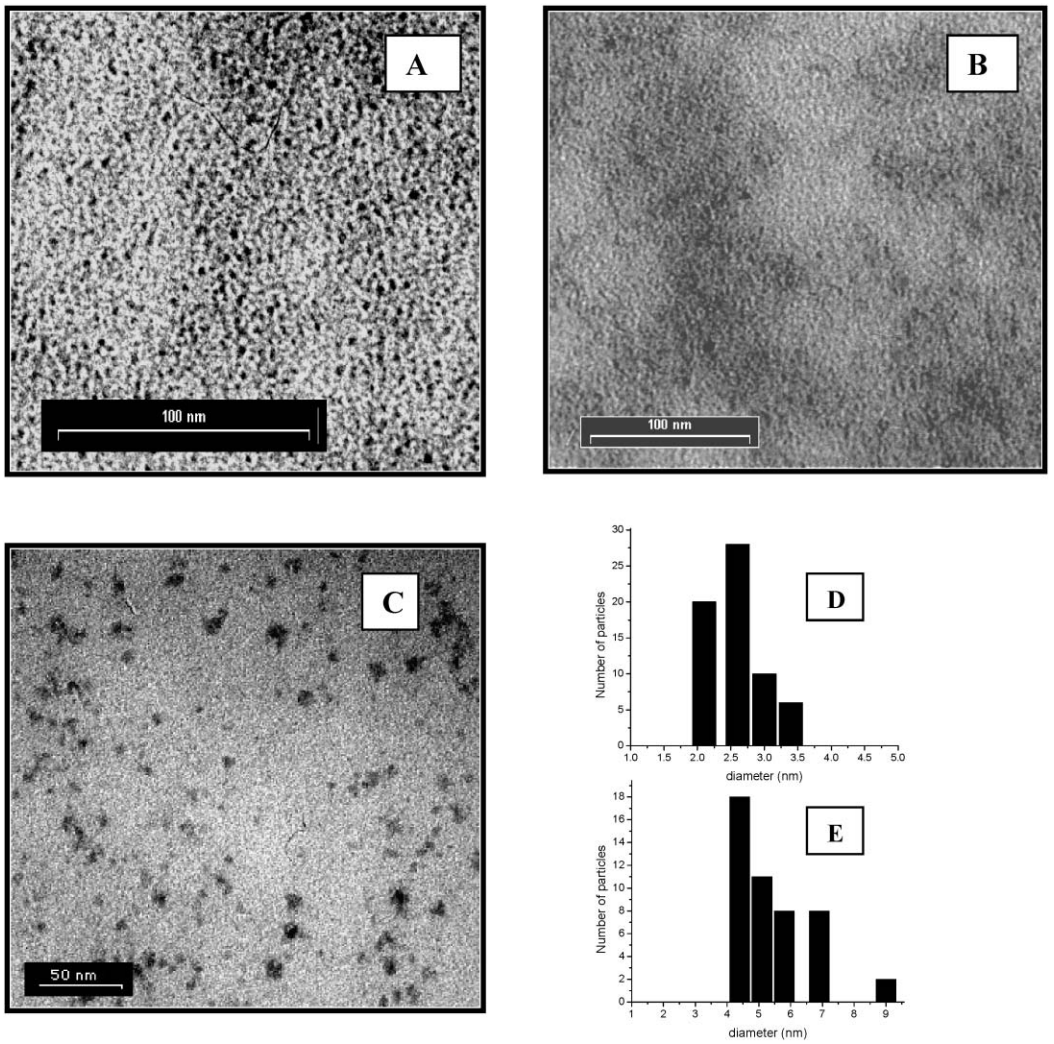

Fig. 7 TEM images of hybrid films functionalized with CdS. (A) CSP3 and (B) CSP5 with 2 mM solutions of $CdCl_2$ and Na_2S. (C) CSP3 with 0.5 mM solutions. (D) Size distribution of the CdS particles in CSP3 with 2 mM (A) and (E) 0.5 mM solutions (C) of $CdCl_2$ and Na_2S. See Table 1 for sample compositions.

of 1 to 10 are classified as favorable adsorptions[52,53] and values of $1/n < 1$ indicate a stronger bond between adsorbate and adsorbent.[54] Thereby, we can conclude that CSP3 film is a good adsorbent for Cd^{2+} ions. This fact is in accordance with the well known capacity of chitosan for Cd^{2+} ion adsorption.[55,56]

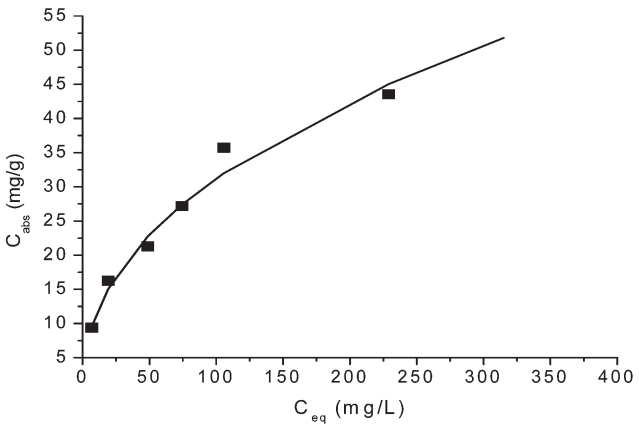

Fig. 8 Adsorption isotherm of cadmium ions by CSP3 hybrid film.

Conclusions

It was possible to synthesize CdS nanoparticles with narrow particle size distribution inside transparent adhesive and insoluble polyelectrolyte films, which are composed of chitosan (CHI), poly(monomethyl itaconate) (PMMI) and silica (SiO_2) in variable amounts in an aqueous environment *via* a simple and upscalable method using cheap and commonly available chemicals. The particle size could be tuned between 3 and 6 nm corresponding to an absorption onset of 435–490 nm. By increasing the CHI amount in the films the absorption edge of the obtained CdS nanoparticles was decreased gradually. The effect of pH and reactant concentration on the optical properties of CdS nanoparticles synthesized *in situ* was also studied. The adsorption capacity of the films can be adjusted *via* a simple pH variation. The results also indicate that a critical value of Cd^{2+} concentration exists above which CdS nanoparticles begin to be formed with a

narrow size distribution. The maximum concentration of CdS nanoparticles synthesized *in situ* is controlled by the adsorption capacity of the films.

Such hybrid films have useful optical properties, as the light absorption spectra of the semiconductor could be tuned *via* the adjustable semiconductor particle size. The hybrid material can be applied as a coating, as the transparent films are adhesive so that the optical properties of CdS can be exploited for example as selective light filters with tunable absorption onset. Advantages of the material are the easy synthesis and the possibility to apply the films in aqueous environment, as the semiconductor nanoparticles do not wash out. We use cheap and commonly available materials for the preparation of semiconductor functionalized organic–inorganic hybrid films and our synthesis can be easily scaled up. In addition, in contrast to recently prepared materials including CdS nanoparticles in a polymer matrix,[57] it is not necessary to introduce capping agents in order to inhibit the aggregation of the particles since the amino groups of chitosan act as passivators of the nanoparticle surface. The high quality monodisperse semiconductor particles are synthesized in a controlled fashion directly within the transparent adhesive polymer film matrix at ambient conditions. It can be expected that this strategy is transferable to a number of other nanoparticles.

Acknowledgements

Financial support by the CONICYT through projects Fondecyt 1050651 and Fondap 11980002 is greatly appreciated.

References

1 H. Weller, *Angew. Chem., Int. Ed. Engl.*, 1993, **32**, 41.
2 A. D. Yoffe, *Adv. Phys.*, 1993, **42**, 173.
3 L. E. Brus, *J. Chem. Phys.*, 1983, **79**, 5466.
4 M. V. R. Krishna and R. A. Friesner, *Phys. Rev. Lett.*, 1991, **67**, 629.
5 P. E. Lippens and M. Lannoo, *Phys. Rev. B*, 1989, **39**, 10935.
6 M. P. Pileni, *Nat. Mater.*, 2003, **2**, 145.
7 S. Kumar and T. Nann, *Small*, 2006, **2**, 316.
8 C. de Mello Donega, P. Liljeroth and D. Vanmaekelbergh, *Small*, 2005, **1**, 1152.
9 L. Qi, H. Cölfen and M. Antonietti, *Nano Lett.*, 2001, **1**, 61.
10 H. Zhang, Z. Cui, Y. Wang, K. Zhang, X. Ji, Ch. Lü, B. Yang and M. Gao, *Adv. Mater.*, 2003, **15**, 777.
11 W. Xu, Y. T. Liao and D. L. Akins, *J. Phys. Chem. B*, 2002, **106**, 11127.
12 S. Wang, P. Liu, X. Wang and X. Fu, *Langmuir*, 2005, **21**, 11969.
13 E. J. C. Dawnay, M. A. Fardad, M. Green and E. M. Yeatman, *J. Mater. Res.*, 1997, **12**, 3115.
14 Y. Wang and W. Mahler, *Opt. Commun.*, 1987, **61**, 233.
15 H. Du, G. Q. Xu and W. S. Chin, *Chem. Mater.*, 2002, **14**, 4473.
16 Y. Yuan, J. H. Fendler and I. Cabasso, *Chem. Mater.*, 1992, **4**, 312.
17 F. M. Pavel and R. A. Mackay, *Langmuir*, 2000, **16**, 8568.
18 N. Herron, Y. Wang and H. Eckert, *J. Am. Chem. Soc.*, 1990, **112**, 1322.
19 T. Vossmeyer, L. Katsikas, M. Giersig, I. G. Popovic, K. Diesner, A. Chemseddinne, A. Eychmueller and H. Seller, *J. Phys. Chem.*, 1994, **98**, 7665.
20 W. T. Yao, S. H. Yu, S. J. Liu, J. P. Chen, X. M. Liu and F. Q. Li, *J. Phys. Chem. B*, 2006, **110**, 11704.
21 W. Sheng, S. Kim, J. Lee, S. W. Kim, K. Jensen and M. G. Bawendi, *Langmuir*, 2006, **22**, 3782.
22 Y. K. Olsson, G. Chen, R. Rapaport, D. T. Fuchs, V. C. Sundara, J. S. Steckel, M. G. Bawendi, A. Aharoni and U. Banin, *Appl. Phys. Lett.*, 2004, **85**, 19.
23 M. Gao, M. Gao, X. Zhang, Y. Yang, B. Yang and J. Shen, *J. Chem. Soc., Chem. Commun.*, 1994, 2777.
24 M. Gao, X. Zhang, B. Yang and J. Shen, *J. Chem. Soc., Chem. Commun.*, 1994, 2229.
25 A. S. Susha, F. Caruso, A. L. Rogach, G. B. Sukhorukov, A. Kornowski, H. Möhwald, M. Giersig, A. Eychmüller and H. Weller, *Colloids Surf., A*, 2000, **163**, 39.
26 E. Cates, M. W. Pitcher and P. A. Bianconi, *Mater. Chem. Phys.*, 2005, **94**, 13.
27 Y. Yang, H. L. Chen and X. M. Bao, *J. Cryst. Growth*, 2003, **252**, 251.
28 S. Radhakrishnan, *J. Cryst. Growth*, 1994, **141**, 437.
29 J. Lin, E. Cates and P. A. Bianconi, *J. Am. Chem. Soc.*, 1994, **116**, 4738.
30 P. A. Bianconi, J. Lin and A. R. Strzelecki, *Nature*, 1991, **349**, 315.
31 F. Antolini, M. Pentimalli, T. Di Luccio, R. Terzi, M. Schioppa, M. Re, L. Mirenghi and L. Tapfer, *Mater. Lett.*, 2005, **59**, 3181.
32 K. G. Kanade, R. R. Hawaldar, R. Pasricha, S. Radhakrishnan, T. Seth, U. P. Mulik, B. B. Kale and D. P. Amalnerkar, *Mater. Lett.*, 2005, **59**, 554.
33 Y. Martínez, J. Retuert, M. Yazdani-Pedram and H. Cölfen, *Polymer*, 2004, **45**, 3257.
34 M. Rinaudo and A. Domard, *Chitin and chitosan: sources, chemistry, physical properties and applications*, Elsevier Science Publishers, Essex, UK, 1989, 71.
35 B. R. Baker, R. E. Shaub and G. H. Wiliams, *J. Org. Chem.*, 1952, **17**, 122.
36 M. Breulmann, H. Cölfen, H. P. Hentze, M. Antonietti, D. Walsh and S. Mann, *Adv. Mater.*, 1998, **10**, 237.
37 A. Henglein, *Chem. Rev.*, 1989, **89**, 1861.
38 A. P. Alivisatos, *J. Phys. Chem.*, 1996, **100**, 13226.
39 M. P. Pileni, L. Motte and C. Petit, *Chem. Mater.*, 1992, **4**, 338.
40 Y.-C. Chua, C.-C. Wangb and C.-Y. Chena, *J. Membr. Sci.*, 2005, **247**, 201.
41 B. I. Lemon and R. M. Crooks, *J. Am. Chem. Soc.*, 2000, **122**, 12886.
42 M. Tamborra, M. Striccoli, R. Comparelli, M. L. Curri, A. Petrella and A. Agostiano, *Nanotechnology*, 2004, **15**, S240.
43 V. K. LaMer and R. H. Dinegar, *J. Am. Chem. Soc.*, 1950, **72**, 4847.
44 M. P. Pileni, *Langmuir*, 1997, **13**, 3266.
45 B. A. Korgel and H. G. Monbouquette, *J. Phys. Chem.*, 1996, **100**, 346.
46 T. Vossmeyer, L. Katzikas, M. Giersig, G. Popovic, K. Diesner, A. Chemseddine, A. Eychmüller and H. Weller, *J. Phys. Chem.*, 1994, **98**, 7675.
47 C. Fischer, H. Weller, L. Katzikas and A. Henglein, *Langmuir*, 1989, **5**, 429.
48 N. Chestoy, T. D. Harris, R. Hull and L. E. Brus, *J. Phys. Chem.*, 1986, **90**, 3393.
49 D. Diaz, M. Rivera, T. Ni, J. C. Rodríguez, S. E. Castillo-Blum, D. Nagesha, J. Robles, O. J. Alvarez-Fregoso and N. A. Kotov, *J. Phys. Chem. B*, 1999, **103**, 9854.
50 G. Carrot, S. M. Scholz, C. J. G. Plummer, J. G. Hilborn and J. L. Hedrick, *Chem. Mater.*, 1999, **11**, 3571.
51 S. Fuentes, J. Retuert, A. Ubilla, J. Fernandez and G. Gonzalez, *Biomacromolecules*, 2000, **1**, 239.
52 M. Rao and A. G. Bhole, *J. Indian Water Works Assoc.*, 2001, **33**, 93.
53 C. Raji, K. P. Shubha and T. S. Anirudhan, *Indian J. Environ. Health*, 1997, **39**, 230.
54 M. Ajmal, A. Mohammad, R. Yousuf and A. Ahmad, *Indian J. Environ. Health*, 1998, **40**, 15.
55 I. N. Jha, L. Iyengar and A. V. S. Prabhakara Rao, *J. Environ. Eng.*, 1988, **114**, 962.
56 B. Benguella and H. Benaissa, *Colloids Surf., A*, 2002, **201**, 143.
57 L. Pedone, E. Caponetti, M. Leone, V. Militello, V. Panto, S. Polizzi and M. L. Saladino, *J. Colloid Interface Sci.*, 2005, **284**, 495.